Investigation of THz birefringence measurement and calculation in Al_2O_3 and $LiNbO_3$

Youngchan Kim,[1] Minwoo Yi,[1] Bog G. Kim,[2] and Jaewook Ahn[1,*]

[1]Department of Physics, KAIST, Daejeon 305-701, South Korea

[2]Department of Physics, Pusan National University, Pusan 609-735, South Korea

*Corresponding author: jwahn@kaist.ac.kr

Received 9 March 2011; accepted 14 April 2011;
posted 29 April 2011 (Doc. ID 143919); published 13 June 2011

Based on the polarization-sensitive terahertz time-domain spectroscopy, we measured the birefringence for Al_2O_3 and $LiNbO_3$ single crystals, which correspond to trigonal structures that have an uniaxial birefringence, in the THz frequency range of 0.25 to 1.4 THz. For more comprehensive understanding of the THz birefringence, the measured birefringence is compared with the results of *ab initio* calculations. The measured birefringence shows good agreement with the calculated value. © 2011 Optical Society of America

OCIS codes: 160.1190, 260.1440, 300.6250, 300.6495.

1. Introduction

With the rapid development of the terahertz (THz) technology, electromagnetic radiations whose frequency locates between the microwaves and infrared light, also known as THz waves, have recently drawn much attention due to their technical applications and fundamental interests [1–4]. In particular, terahertz time-domain spectroscopy (THz-TDS) has become one of the essential analyzing tools in material science. Many materials have complex dielectric responses in the frequency range of 0.1 to 10 THz, and advanced optical properties, such as birefringence, and magneto/electro-optical effects in the THz frequency range are under active investigation by using THz-TDS [5–7]. The potential application of THz systems is particularly promising for high-speed communications, biological and medical investigation, secure inspection, and hazardous material detection. [4,8–10].

Aluminum oxide is a family of inorganic compounds, an amphoteric oxide with the chemical formula Al_2O_3, which has a unique combination of outstanding chemical, physical, and optical properties: Al_2O_3 crystal has a high mechanical strength at high temperatures, good thermal properties, and excellent optical transparency [11]. Its mechanical properties begin to decline after 800 °C. Moreover, it is an electrical insulator but has a high thermal conductivity ($30\,Wm^{-1}\,K^{-1}$) for a ceramic material [11]. Thus, Al_2O_3 is of general and extensive use for a substrate for many epitaxial films as well as for a protected window from the vacuum ultraviolet to the infrared spectrum range. Lithium niobate ($LiNbO_3$) is one of the most attractive materials for optoelectronics, due to its excellent electro-optic, acousto-optic, and nonlinear optical properties [12]. $LiNbO_3$ has good chemical and mechanical stabilities and is transparent over a wide frequency range. Applications include electro-optic modulators in mobile phones, and *Q*-switchers for Nd:YAG, Nd:YLF, and Ti:sapphire lasers, as well as guided optical modulators for fiber optics.

In this study, we present measurements of the extraordinary and ordinary refractive indices (n_e and n_o) of Al_2O_3 and $LiNbO_3$ single crystals in the frequency range of 0.25–1.40 THz. The THz birefringence ($\Delta n = n_e - n_o$) is measured using a THz-TDS, which is used to enable polarization-sensitive THz detection, demonstrated previously with liquid crystal polymers, natural products, and crystals, such as

0003-6935/11/182906-05$15.00/0

rutile and zinc oxide [13–15]. The results are comparable with the earlier FT-THz measurements [16,17]. For more comprehensive understanding of the THz birefringence of the investigated materials, we compare our experimental results with the calculated results obtained using an *ab initio* phonon calculation using CRYSTAL09 code [18].

2. Polarization-Sensitive Terahertz Detection

The experimental configuration is illustrated in Fig. 1. A pump beam, the subpicosecond infrared (800 nm) pulses from a Ti:sapphire laser oscillator, was incident on the THz emitter, which was the biased photoconductive antenna (PCA). The pulsed THz waves polarized linearly along the vertical axis were generated from the PCA and focused on the sample with a spot size of ~2 mm. Then the THz waves transmitted through the sample were guided into the ZnTe crystal overlapping with the linearly polarized probe beam along the horizontal axis by using four off-axis parabolic mirrors. The enclosure containing the THz beam path was purged with nitrogen gas to eliminate the absorption by water vapor in ambient air. After the ZnTe crystal, the probe beam passed through a quarter wave plate and was split by a Wollaston prism into the two orthogonal polarization components, which were then respectively sent to two detectors. The intensity difference measured from the detectors between the two orthogonal polarization components was proportional to the detected THz field amplitude E_{THz}.

In the theoretical calculation [19], the intensity difference is given by

$$\Delta I(\alpha,\varphi) = I_P \frac{\omega n^3 E_{\mathrm{THz}} r_{41} L}{2c} (\cos\alpha \sin 2\varphi + 2\sin\alpha\cos 2\varphi), \quad (1)$$

where I_P is the probe beam intensity, ω is the angular frequency of the probe beam, n is the refractive index of ZnTe, c is the speed of light in vacuum, r_{41} and L are the only nonzero coefficient of the electro-optic tensor and the thickness of the ZnTe, respectively. As shown in the inset at top right of Fig. 1, α and φ are the angles of the THz and probe beam polarizations with respect to the (001) axis of ZnTe, respectively. In our experimental condition, the angle of THz polarization is perpendicular to that of the probe beam polarization ($\varphi = \alpha + 90°$).

Figure 2 shows the measured THz time-domain waveforms as a function of the THz polarization angle α from 0° to 360° at a step of 10° with respect to the (001) axis of ZnTe when the probe beam polarization angle φ is fixed at 180°. It can be found from Eq. (1) that, ignoring the sign of THz amplitude, there are the two absolute maxima of the THz amplitude at the THz polarization angles α of 90° and 270°. Using this polarization-sensitive THz-TDS, we measured the THz refractive indices for Al_2O_3 and $LiNbO_3$ crystals according to an azimuthal angle θ, rotating them placed on the focal plane, as shown in Fig. 1.

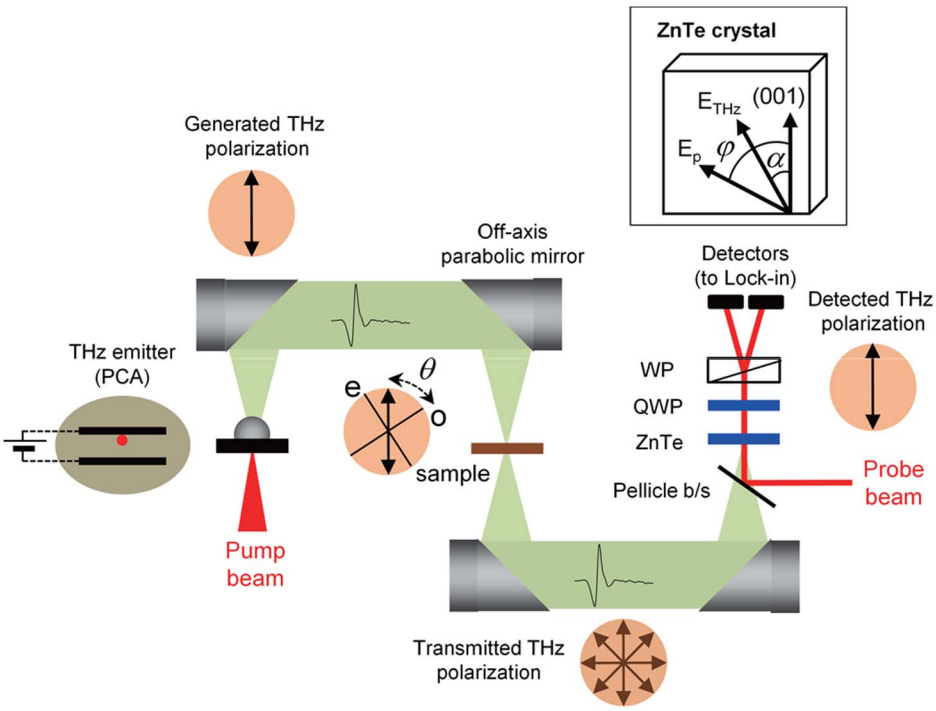

Fig. 1. (Color online) Illustration of the experimental configuration. PCA, photoconductive antenna; WP, Wollaston prism; QWP, quarter waveplate; Pellicle b/s, Pellicle beamsplitter; o, ordinary axis; and e, extraordinary axis. The directions of the generated and detected THz polarizations are depicted beside the THz emission and detection parts, respectively. The inset shows the angles of the THz and probe beam polarization directions with respect to the (001) axis of the ZnTe crystal.

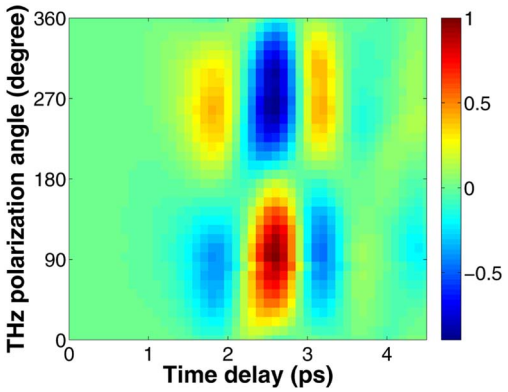

Fig. 2. (Color online) THz polarization-dependent THz time-domain waveforms (arbitrary units) measured with varying the THz polarization angle α with respect to the (001) axis of the ZnTe crystal.

3. Measurement of the Terahertz Birefringence

The samples are prepared both-side polished with 0.5 mm thickness. The (10–10) crystal orientation was prepared for Al_2O_3, and x-cut for $LiNbO_3$. We note that both Al_2O_3 and $LiNbO_3$ crystals correspond to the trigonal structures having a uniaxial birefringence.

The reference and transmitted temporal waveforms of THz pulses, which were measured over 34 ps in time-domain data, were recorded with and without the samples, respectively. Figure 3 displays the transmitted THz waveforms, which are measured by rotating the $LiNbO_3$ from 0 to 360° at a step of 5° in the THz-TDS that is described above and illustrated in the inset at top right of Fig. 3. The transmitted THz waveforms of Al_2O_3 were also measured (data not shown). The time delay position of the THz pulse oscillates with a 180° period of the azimuthal angle θ, which implies the existence of birefringence. From the result of Fig. 3, we can characterize the crystal orientation of the Al_2O_3 crystal without *a priori* knowledge of the crystal orientation. For a given crystal orientation, the index of refraction of

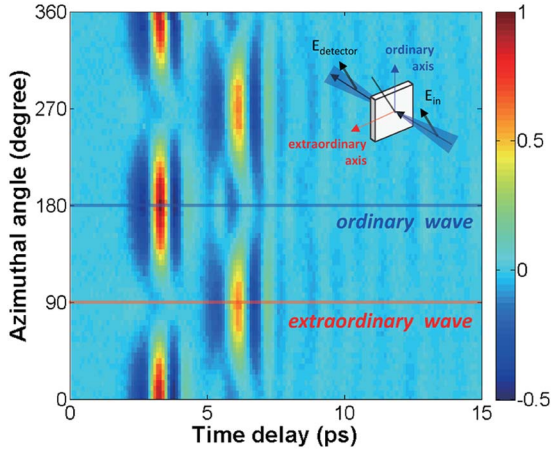

Fig. 3. (Color online) Transmitted THz time-domain waveforms (arbitrary units) measured with varying the azimuthal angle θ of the $LiNbO_3$.

the sample is obtained by comparing the THz waveform measurements with and without the sample [20]. Briefly, the ratio between the reference and transmitted THz spectra is given by (for the notation, see Fig. 4)

$$\frac{\tilde{E}_{\text{sample}}(\omega)}{\tilde{E}_{\text{reference}}(\omega)} = \frac{\tilde{n}_s(\omega)(\tilde{n}_1+\tilde{n}_2)(\tilde{n}_2+\tilde{n}_3)}{\tilde{n}_2(\tilde{n}_1+\tilde{n}_s(\omega))(\tilde{n}_s(\omega)+\tilde{n}_3)} \times e^{-i(\tilde{n}_s(\omega)-\tilde{n}_2)\omega L/c} = \rho(\omega)e^{-i\phi(\omega)}, \quad (2)$$

where $\rho(\omega) = \left|\frac{\tilde{E}_{\text{sample}}(\omega)}{\tilde{E}_{\text{reference}}(\omega)}\right|$ and $\varphi(\omega) = \arg\left(\frac{\tilde{E}_{\text{sample}}(\omega)}{\tilde{E}_{\text{reference}}(\omega)}\right)$. For a sample with very low absorption, and $\tilde{n}_1 = \tilde{n}_2 = \tilde{n}_3 = 1$, the frequency-dependent real part of the complex refractive index of the sample, $n_s(\omega)$, is given by

$$n_s(\omega) = 1 + \frac{c\varphi(\omega)}{\omega d}, \quad (3)$$

where d is the crystal thickness and c is the speed of light.

Figure 5 shows the measured dispersion of extraordinary and ordinary refractive indices (n_e and n_o) for the Al_2O_3 and $LiNbO_3$ samples.

4. Calculation for Terahertz Birefringence

For more comprehensive understanding of THz birefringence, the measured birefringence is compared with the result of *ab initio* calculations. We carried out an *ab initio* phonon calculation using CRYSTAL09 [18], which employed a hybrid exchange-correlation functional PBE0 [21] and a localized basis set of Gaussian-type functions of oxygen (6-31d1) and aluminum (8-511d1) for Al_2O_3 and Lithium (6-11G) and Haywsc pseudopotential of niobium (Haywsc-31d) and oxygen (6-31d1) for $LiNbO_3$ [22]. Starting from experimentally known trigonal space group (R-3c, No. 167 for Al_2O_3 and R3c, No. 161 for $LiNbO_3$) [23], internal coordinates of each atom and lattice parameters are varied to minimize the total energy for a given symmetry. Then the coupled perturbed Kohn–Sham equation has been

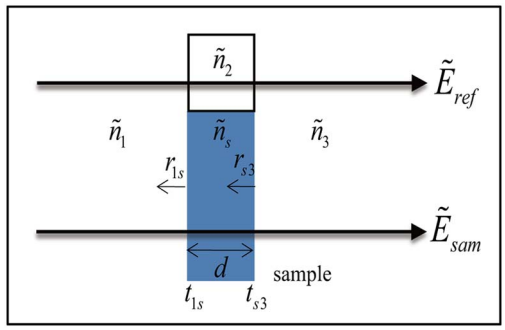

Fig. 4. (Color online) Measurement of THz waveforms with and without the sample. The frequency-dependent refractive index of the sample, $\tilde{n}_s(\omega)$, is obtained from Eqs. (2) and (3).

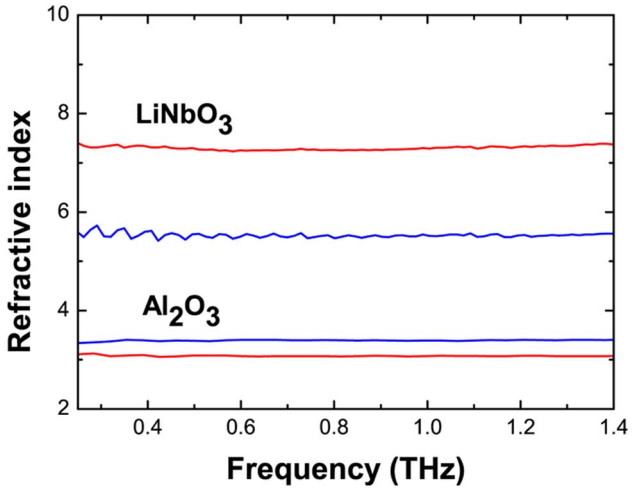

Fig. 5. (Color online) Dispersion of measured ordinary and extraordinary refractive indices of Al_2O_3 and $LiNbO_3$. The extraordinary and ordinary waves are indicated by the red and blue curves, respectively.

solved for each optimized structure in order to obtain dielectric function at optical frequencies [24]. Finally, a full phonon calculation has been carried out to obtain the phonon spectrum at the zone center [25]. The calculated phonon spectrum including longitudinal and transverse phonon has been used to obtain the frequency-dependent dielectric constant in the THz region.

Figure 6 shows the calculated refractive indices of Al_2O_3 and $LiNbO_3$ with respect to the two different polarizations, which are the result from the *ab initio* calculation: the extraordinary and ordinary refractive indices. The measured and calculated refractive indices of the Al_2O_3 and $LiNbO_3$ at 1 THz are listed in Table 1. Our *ab initio* calculation reproduces the experimental results quite well as listed in Table 1, as well as the FT-THz measurements in [16,17].

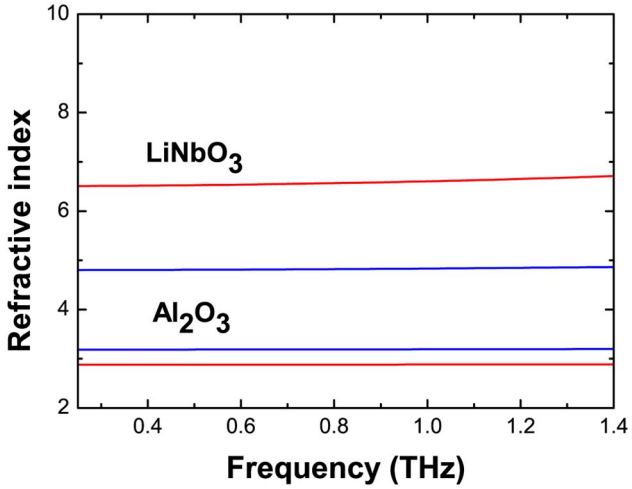

Fig. 6. (Color online) Dispersion of calculated ordinary and extraordinary refractive indices of Al_2O_3 and $LiNbO_3$ by using an *ab initio* calculation. The extraordinary and ordinary waves are indicated by the red and blue curves, respectively.

Table 1. Measured and Calculated Refractive Indices of Al_2O_3 and $LiNbO_3$ at 1 THz

Refractive Index at 1 THz	Al_2O_3			$LiNbO_3$		
	n_e	n_o	Δn	n_e	n_o	Δn
Measurement	3.07	3.39	−0.32	7.29	5.51	1.78
Calculation	2.88	3.19	−0.31	6.60	4.83	1.77
Reference [16,17]	3.09	3.41	−0.32	6.72	5.09	1.63

5. Conclusion

In conclusion, we have studied the THz birefringence of Al_2O_3 and $LiNbO_3$, which correspond to the trigonal structures that have a uniaxial birefringence. Using a polarization-sensitive THz-TDS, we measured the extraordinary and ordinary refractive indices of the Al_2O_3 and $LiNbO_3$ in the frequency range of 0.25 to 1.40 THz. The experimental results of the THz birefringence for the samples show good agreement with the results of a model considering phonon contributions. Therefore, the birefringence for the sample in the THz frequency region can be well understood in conjunction with the phonon consideration.

The authors thank the referee for the helpful comments and acknowledge the support from National Research Foundation of Korea (NRF) funded by the Ministry of Education, Science, and Technology (2010-0013899, 2009-0090843, 2010-0001226 and 2010-0002405).

References and Notes

1. Y.-S. Lee, *Principles of Terahertz Science and Technology* (Springer, 2009).
2. B. Ferguson and X.-C. Zhang, "Materials for terahertz science and technology," Nat. Mater. **1**, 26–33 (2002).
3. B. E. Cole, J. B. Williams, B. T. King, M. S. Sherwin, and C. R. Stanley, "Coherent manipulation of semiconductor quantum bits with terahertz radiation," Nature **410**, 60–63 (2001).
4. M. Tonouchi, "Cutting-edge terahertz technology," Nat. Photon. **1**, 97–105 (2007).
5. M. van Exter, Ch. Fattinger, and D. Grischkowsky, "Terahertz time-domain spectroscopy of water vapor," Opt. Lett. **14**, 1128–1130 (1989).
6. K. Kawase, Y. Ogawa, Y. Watanabe, and H. Inoue, "Non-destructive terahertz imaging of illicit drugs using spectral fingerprints," Opt. Express **11**, 2549–2554 (2003).
7. M. Brucherseifer, M. Nagel, P. H. Bolivar, H. Kurz, A. Bosserhoff, and R. Büttner, "Label-free probing of the binding state of DNA by time-domain terahertz sensing," Appl. Phys. Lett. **77**, 4049–4051 (2000).
8. T. Kleine-Ostmann and T. Nagatsuma, "A review of terahertz communications research," J. Infrared Milli. Terahz. Waves **32**, 143–171 (2011).
9. P. H. Siegel, "Terahertz technology in biology and medicine," IEEE Trans. Microwave Theory Tech. **52**, 2438–2447 (2004).
10. Y. C. Shen, T. Lo, P. F. Taday, B. E. Cole, W. R. Tribe, and M. C. Kemp, "Detection and identification of explosives using terahertz pulsed spectroscopic imaging," Appl. Phys. Lett. **86**, 241116 (2005).
11. http://www.makeitfrom.com/data/?material=Alumina.

12. S. Kojima, N. Tsumura, H. Kitahara, M. W. Takeda, and S. Nishizawa, "Terahertz time domain spectroscopy of phonon-polaritons in ferroelectric lithium niobate crystals," Jpn. J. Appl. Phys. **41**, 7033–7037 (2002).
13. F. Rutz, T. Hasek, M. Koch, H. Richter, and U. Ewert, "Terahertz birefringence of liquid crystal polymers," Appl. Phys. Lett. **89**, 221911 (2006).
14. C. Jordens, M. Scheller, M. Wichmann, M. Mikulics, K. Wiesauer, and M. Koch, "Terahertz birefringence for orientation analysis," Appl. Opt. **48**, 2037–2044 (2009).
15. Y. Kim, J. Ahn, B. G. Kim, and D.-S. Yee, "Terahertz birefringence in zinc oxide," Jpn. J. Appl. Phys. **50**, 030203 (2011).
16. E. D. Palik, *Handbook of Optical Constants of Solids II* (Academic, 1985), p. 765.
17. E. D. Palik, *Handbook of Optical Constants of Solids I* (Academic, 1985), p. 700.
18. R. Dovesi, V. R. Saunders, C. Roetti, R. Orlando, C. M. Zicovich-Wilson, F. Pascale, B. Civalleri, K. Doll, N. M. Harrison, I. J. Bush, Ph. D'Arco, and M. Llunell, CRYSTAL09 User's Manual (University of Torino, 2009).
19. P. C. M. Planken, H.-K. Nienhuys, H. J. Bakker, and T. Wenckebach, "Measurement and calculation of the orientation dependence of terahertz pulse detection in ZnTe," J. Opt. Soc. Am. B **18**, 313–317 (2001).
20. S. P. Mickan and X.-C. Zhang, "T-ray sensing and imaging," Int. J. High Speed Electron. Syst. **13**, 601–676 (2003).
21. C. Adamo and V. Barone, "Toward reliable density functional methods without adjustable parameters: the PBE0 model," J. Chem. Phys. **110**, 6158–6170 (1999).
22. http://www.crystal.unito.it/Basis_Sets/Ptable.html.
23. ICSD (International Crystal Structure database) website, ID 5674 for Al_2O_3 and ID 11588 for $LiNbO_3$.
24. M. Ferrero, M. Rérat, R. Orlando, and R. Dovesi, "Coupled perturbed Hartree-Fock for periodic systems: the role of symmetry and related computational aspects," J. Chem. Phys. **128**, 014110 (2008).
25. C. M. Zicovich-Wilson, F. J. Torres, F. Pascale, L. Valenzano, R. Orlando, and R. Dovesi, "Ab initio simulation of the IR spectra of pyrope, grossular and andradite," J. Comput. Chem. **29**, 2268–2278 (2008).